

CrystEngComm

Accepted Manuscript



This is an *Accepted Manuscript*, which has been through the Royal Society of Chemistry peer review process and has been accepted for publication.

Accepted Manuscripts are published online shortly after acceptance, before technical editing, formatting and proof reading. Using this free service, authors can make their results available to the community, in citable form, before we publish the edited article. We will replace this *Accepted Manuscript* with the edited and formatted *Advance Article* as soon as it is available.

You can find more information about *Accepted Manuscripts* in the [Information for Authors](#).

Please note that technical editing may introduce minor changes to the text and/or graphics, which may alter content. The journal's standard [Terms & Conditions](#) and the [Ethical guidelines](#) still apply. In no event shall the Royal Society of Chemistry be held responsible for any errors or omissions in this *Accepted Manuscript* or any consequences arising from the use of any information it contains.



Journal Name

ARTICLE

Observation of anatase nanograins crystallizing from anodic amorphous TiO₂ nanotubes

Received 00th January 20xx,
Accepted 00th January 20xx

DOI: 10.1039/x0xx00000x

www.rsc.org/

Ik Jae Park,^a Dong Hoe Kim,^a Won Mo Seong,^a Byung Suh Han,^a Gill Sang Han,^b Hyun Suk Jung,^b Mengjin Yang,^c Wen Fan,^d Sangwook Lee,^{*d} Jung-Kun Lee^{*c} and Kug Sun Hong^a

A mechanism underlying appearance of preferred-orientation in anodized amorphous TiO₂ nanotube arrays (NTAs) was studied. Transmission electron microscopic analyses of preferred-oriented nanotube arrays (p-NTAs) reveal that at an optimum water content (~2 wt%), large single crystalline domains oriented along <001> grow into the inner wall from the outer wall to minimize the surface energy. In stark contrast, excessive water content (5 wt%) in the electrolyte leads to sporadic multiple nucleation of randomly-oriented anatase crystallites in amorphous medium at the early stage of crystallization, which result in formation of randomly-oriented nanotube arrays (r-NTAs). During subsequent thermal annealing, multiple nucleation sites hindered the growth of the <001>-oriented grains from the outer wall. When the water content in ethylene glycol-based electrolyte is optimized by reducing the uncertainty of water content, x-ray diffraction patterns of NTAs exhibited 200 times increase in intensity ratio of (004) to (200) peaks of the anatase phase. p-NTAs exhibit ~5 times lower electrical resistance than r-NTAs, which supports that improving preferred orientation of NTA is a promising way for developing efficient electronic devices.

1. Introduction

Over a decade, an anodization method has been used as a simple way to prepare one-dimensional (1-D) nanoporous structures in many material systems such as Al₂O₃,^{1,2} Ta₂O₅,^{3,4} Nb₂O₅,^{5,6} WO₃,⁷ and TiO₂.^{8,9} TiO₂ nanotube arrays (TiO₂-NTAs) are well-known metal oxide materials that have intriguing optical and electronic properties.¹⁰ Since Macak *et al.* reported TiO₂-NTAs with a high aspect ratio and smooth surface,¹¹ TiO₂-NTAs have been considered promising materials that can contribute to nanoporous semiconductor-based solar cells,¹² water splitting systems,¹³ lithium-ion batteries,¹⁴ and sensors.¹⁵

NTAs are expected to pave a way toward superior charge transport by improving both carrier diffusion and collection,¹⁶ resolving the problem resulted from not enough surface area of the 1-D single crystal nanowire. Indeed, the charge transport of conventional NTAs is not as good as theoretically predicted.¹⁷⁻¹⁹ This was a bottle-neck to realize efficient energy conversion devices, for example, dye-sensitized solar cells.²⁰

To overcome this limitation, the microstructure of NTAs needs to be engineered. Recently, many researchers have tried to develop large grains in TiO₂ nanostructures,^{21,22} such as the confined crystallization with anisotropic grain growth in ALD-grown TiO₂ nanotubes.²³ However, there have been a few works reporting the single-crystal or preferred-orientated TiO₂-NTAs grown by anodization method. Zhao *et al.* reported single-crystal anatase NTAs which were obtained via anodization of Ti metal in HF-added H₃PO₄ electrolyte and subsequent annealing.²⁴ However, the length of the single-crystal nanotubes is less than 1 μm, and their formation mechanism is not clearly understood. Jung *et al.* reported few micrometer-long, single-crystal-like, anatase NTAs, which were synthesized via surfactant-assisted anodization in an ethylene glycol-based electrolyte and subsequent annealing.²⁵ In that work, however, the role of the additives, *i.e.* poly(vinyl pyrrolidone) and acetic acid, on the evolution of the single-crystal-like NTAs is not well explained and the origin of the preferred orientation is still veiled. Our recent work on successful synthesis of preferred orientated anatase NTA without any surfactant may offer a clue to explaining the mechanism for the preferred orientation.²⁶ We reported that both the NTAs with the preferred orientation (p-NTAs) and randomly-oriented NTAs (r-NTAs) could be obtained at certain water contents (~2 wt% and ~5 wt%, respectively) in ethylene glycol-based electrolyte for anodization. The quantity of hydroxyl group in NTA, which was injected into amorphous NTAs during anodization, was suggested to cause the preferred orientation of annealed NTAs. The amount of water which is a source of oxygen for the anodization process is

^a Department of Materials Science & Engineering, Seoul National University, Seoul 151-744, Korea.

^b School of Advanced Materials Science & Engineering, Sungkyunkwan University, Suwon 440-746, Korea.

^c Department of Mechanical Engineering and Materials Science, University of Pittsburgh, Pittsburgh, PA 15261, USA.

^d Department of Materials Science and Engineering, University of California at Berkeley, CA 94720, USA.

Electronic Supplementary Information (ESI) available: TEM images of as-grown NTAs and annealed NTAs, SEM image and XRD patterns of an anodized sample grown in 0 wt% water content electrolyte. See DOI: 10.1039/x0xx00000x

expected to control the quantity of a hydroxyl group injected into the metal oxide.²⁷⁻²⁹ However, detailed crystallization mechanisms of amorphous NTAs containing different hydroxyl group contents are still unknown.

In this paper, we investigate further the effect of water content on the crystallization of NTAs during post-annealing with an emphasis on the initial stage of the crystallization process. Our results show the crystallization path from the amorphous NTAs to the anatase NTAs with or without the preferred orientation. A nucleation behavior of anatase domains from an amorphous matrix is very different between p-NTA and r-NTA. Transmission electron microscopic (TEM) analyses of p-NTAs reveal that the crystallization of the anatase phase starts at the outer wall of amorphous NTAs. However, increase in the water content disrupts continuity of nuclei formed in the initial stage of the crystallization by promoting the homogeneous nucleation. Uniformly distributed nuclei between outer and inner wall surfaces impede growth of {004}-oriented domains from the outer wall surface. When water content in ethylene glycol and subsequent heat-treatment are precisely controlled, it is found that 1.5 - 2.5 wt% of water in the electrolyte is an optimum condition for highly (004)-oriented NTAs. Current-voltage (*I-V*) curves measured by conductive atomic force microscope (c-AFM) show that the p-NTA obtained from the optimum condition has nearly 5 times lower electrical resistance than the r-NTA.

2. Experimental

2.1. Preparation of TiO₂ nanotube arrays

Amorphous TiO₂ NTAs were synthesized by anodization method. We found recently that the initial surface roughness of Ti plate is very important to obtain a high preferred orientation.³⁰ Thick Ti plates (2 mm thickness, 99.7%, Sigma Aldrich) were sequentially ground using 320, 400, 600, and 800-grit silicon carbide (SiC) paper (Allied) under streaming water, and then polished for 20 min using an auto-polisher (250 rpm; LaboPol-5, Struers) with a 3 μm diamond suspension (polycrystalline, water-based, Allied). The final Ti plates had mirror-like surfaces. Prepared Ti metal was degreased sequentially with acetone, ethyl alcohol, and distilled water. The electrolyte consisted of ethylene glycol (99.8%, anhydrous, Sigma Aldrich), 0.25 wt% NH₄F (98+%, Sigma Aldrich) and desired amount of water (~1 wt% to ~10 wt%, *i.e.* ~1.11 vol% to ~11.0 vol%, respectively). The initial pH of electrolyte was 6.90, 6.75, and 6.72, when 0 wt%, 2 wt%, and 5 wt% of water was added. To precisely control the amount of water in electrolyte, we first evaporated ethylene glycol to remove water impurity in as-received ethylene glycol before water was added. NH₄F was kept in an Ar-filled glove box. Anodizing reactions were carried out at 15 °C for 2 hr in N₂ atmosphere to prevent water from infiltrating into the electrolyte. Ti substrate and Pt plate were used as a working electrode and a counter electrode. Distance and electric voltage between electrodes were 6 cm and 50 V. Generally, the applied anodization voltage is one of the most important variables

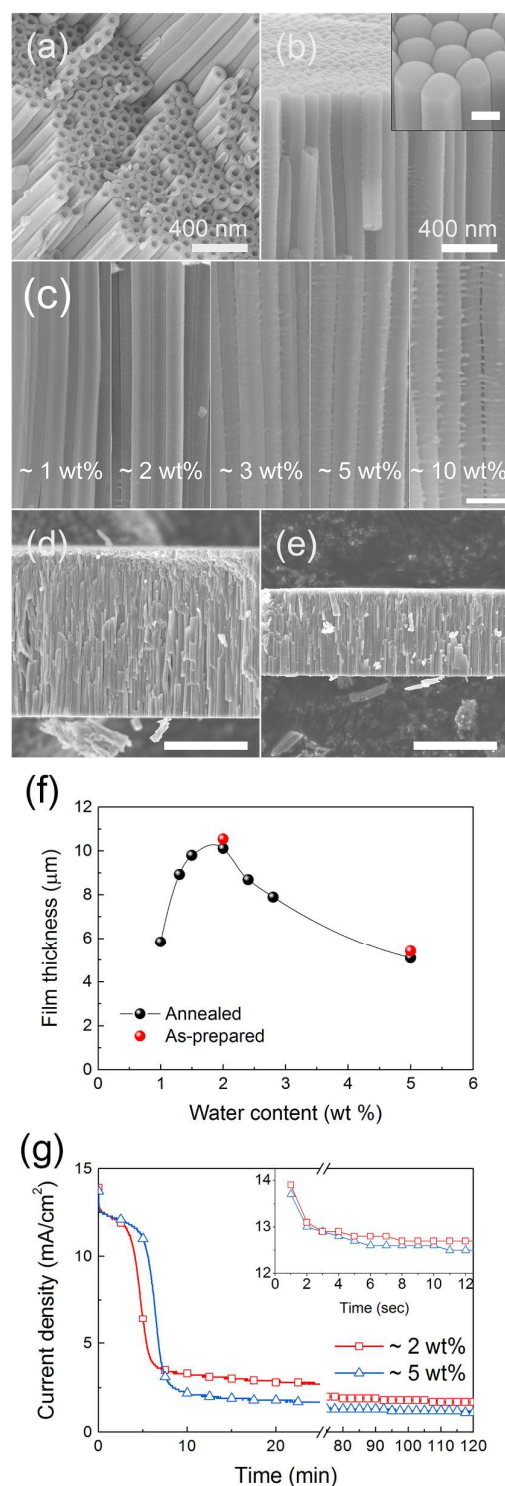


Fig. 1. (a-b) SEM images of the as-grown TiO₂ NTAs (~2 wt%) showing top (a), and side views (b). The inset of (b) shows the high magnification bottom view of the NTAs (scale bar: 100 nm). (c) SEM images of side view of the NTAs grown with various water contents (scale bar: 200 nm). (d-e) The cross-sectional SEM images of the 2W-NTAs (d) and 5W-NTAs (e). Anodization time is 2 hr (scale bar: 5 μm). (f) Length of nanotubes as a function of the water content, after 2 hr of reaction. Annealing induced slight shrinkage (~500 nm) of film thickness of the NTAs. (g) Current density versus time plot of the NTAs. Inset magnifies the initial stage of anodization.

which affect the morphology and the phase of NTAs.^{31,32} We fixed anodization voltage in this study to rule out the effects of the applied voltage on the evolution of morphology and preferred orientation of NTAs. The effect of the applied voltage can be investigated in the future with well-designed, systematic experiments. As-grown NTAs were rinsed using distilled water and ethyl alcohol followed by drying with N₂ stream for a few second until the color of NTAs become bright, and annealed at 450 °C for 1 hr in air (ramp up rate: 2.5 °C/min) to obtain fully crystallized anatase phase.

2.2. Characterization

To investigate morphology of NTAs, samples were examined using field-emission scanning electron microscopy (FESEM, SU70, Hitachi). X-ray diffraction (XRD) patterns were collected to identify the phase and orientation of NTAs (D8, Bruker Miller Co.). A rocking curves of the diffraction peak of (004)-plane ($2\theta = 37.8^\circ$) were also obtained using a different X-ray diffractometer (X'pert PRO, PANalytical). The detailed crystal structure and morphology of the NTAs were studied with high resolution TEM (HRTEM, JEM-3000F, JEOL). *I-V* curve was measured for an individual nanotube to calculate the resistance of the nanotube using c-AFM (Multiview-100, Nanonics). For c-AFM measurement, surface of AFM tip was coated with Pt film. Electric current passing through Pt film was amplified and converted to electric voltage using a current amplifier (DLPCA-200, Femto).

3. Results and Discussion

Vertically oriented TiO₂ NTAs were grown on Ti substrates by anodization in ethylene glycol based organic electrolyte. Morphology of as-grown NTAs from the electrolyte of ~2 wt% water (2W-NTA) is shown in Fig. 1a-b. A diameter of the as-grown NTAs is 130~150 nm and their wall thickness is about 50 nm. There is no significant dependency of the tube diameter on the water content. However, the water content changes the morphology of wall surface and the length of NTAs. Fig. 1c shows the wall surface of the as-grown NTAs from the electrolyte with different water content. The surface of the NTAs from low water content conditions is very smooth without ribs, while the surface of NTAs grown in the electrolyte containing > 5 wt% water is covered with many ribs. 2W-NTAs (~10 μm) is two times as long as 5W-NTAs (NTAs grown in ~5 wt% water), as shown in Fig. 1d-e. These different surface morphology and growth rate of NTAs are due to two different roles of water in the anodization process: i) a source of oxygen and ii) an etchant of fluorine. During NTA formation, H₂O forms the amorphous titanium oxide layer ($2\text{H}_2\text{O} \rightarrow \text{O}_2 + 4\text{e}^- + 4\text{H}^+$, and $\text{Ti} + \text{O}_2 \rightarrow \text{TiO}_2$) which HF subsequently etches out to produce holes (*i.e.* inner walls of NTAs) through electric-field-assisted dissolution ($\text{TiO}_2 + 6\text{F}^- + 4\text{H}^+ \rightarrow \text{TiF}_6^{2-} + 2\text{H}_2\text{O}$). Then, residual fluorine ions (F⁻) near the holes migrate into the side walls of the holes faster than oxygen ion (O²⁻) or hydroxyl ion (OH⁻) and accumulate in the

middle region between the etched holes.³³ Later, this fluorine concentrated region is

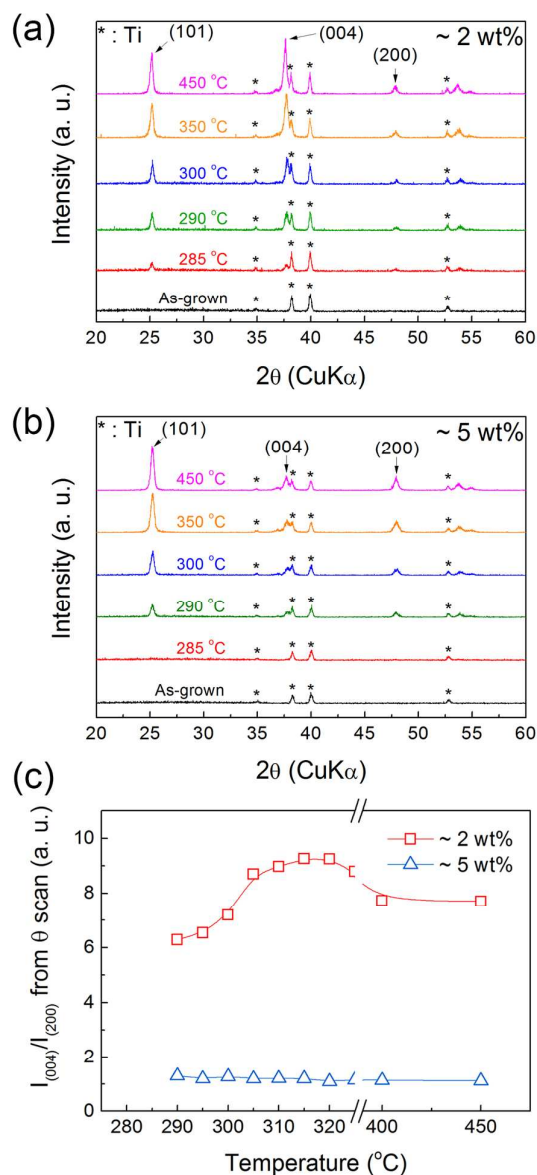


Fig. 2. (a-b) In-situ XRD results taken with varying temperature from the 2W-NTAs (a) and 5W-NTAs (b). (c) XRD peak intensity ratio, $I_{(004)}/I_{(200)}$, as the function of temperature, obtained from the in-situ XRD results.

etched out by water ($\text{TiF}_4 + 2\text{H}_2\text{O} \rightarrow \text{H}^+ + [\text{TiF}_4(\text{OH})\text{H}_2\text{O}]$), leading to the formation of outer pores. The NTA formation mechanism indicates that an increase in water content makes the etching of outer pore faster than that of inner pore, due to the role of water as the etchant of the outer pore. This disparity in the etching rate of inner and outer pores is an origin of the ribs observed on the outer surface of NTAs grown in the electrolyte with the high water content.³⁴

In addition to the different surface morphology, an increase in the water content over 2 wt% decreases the growth rate of

NTAs, as shown in Fig. 1f. To examine a change in the growth rate, the electric current flow of the anodization process was

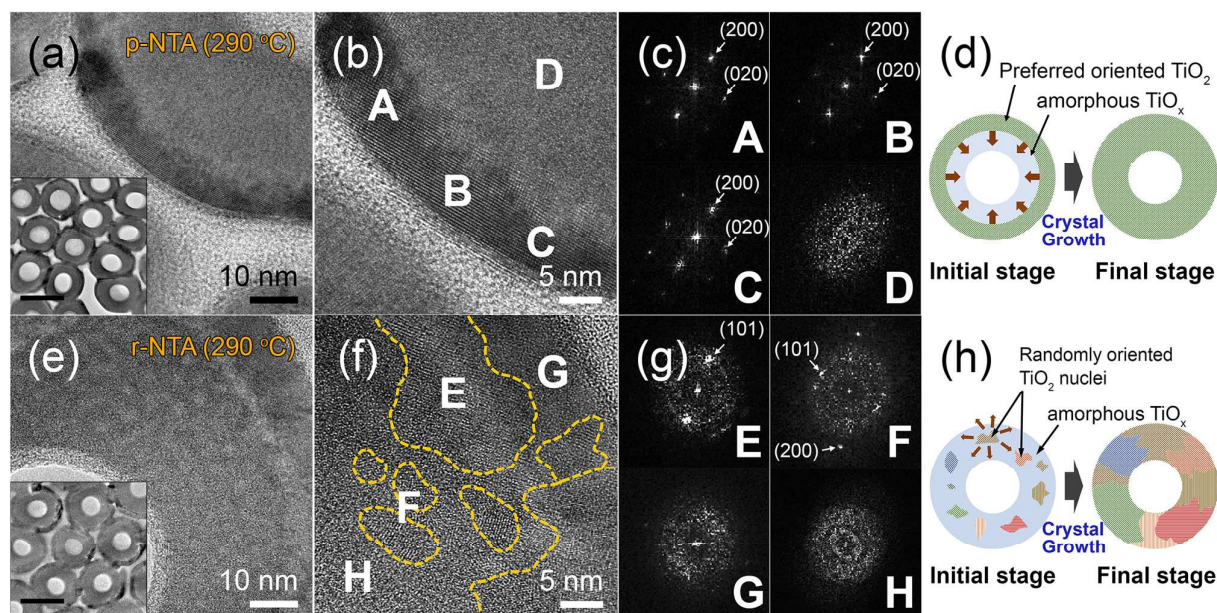


Fig. 3. The cross-sectional TEM images of partially crystallized (anatase-amorphous mixed) (a, b) p-NTAs and (e, f) r-NTAs obtained by annealing at 290 °C for 1 hr. The inset of (a, e) are low magnification images of the p-NTAs and r-NTAs (scale bar: 100 nm). (c, g) are FFT patterns obtained at each partial region (A-H) in (b, f). The yellow dashed region marked in (f) show the randomly oriented crystal grains. (d, h) show schematic diagrams of crystal growth mechanism for p-NTA and r-NTA.

monitored as a function of the reaction time (Fig. 1g). Overall feature of the current density-time curves of the anodization processes in ~2 wt% and ~5 wt% H₂O look similar. Rapid current drop at the most initial stage (<a few seconds) magnified in an inset of Fig. 1g, is a proof of the oxide layer formation on the surface of the Ti substrate.^{35,36} In a next stage, the electric current is constantly maintained for a few hundreds of sec in the ~2 wt% and ~5 wt% H₂O (the second stage), indicating that nanopores are being created from the surface of the oxide layer.³⁶ Longer time for the pore formation at the initial stage, and lower saturation current density at the later stage in ~5 wt% H₂O electrolyte imply that a thicker anodic oxide layer is formed in the electrolyte with the higher water content, agreed with literatures.³⁴ Consequently, as the water content in the electrolyte increases, the electric field across the oxide film, which is a driving force of the pore channel growth in the anodic oxide layer, becomes weaker, and hence the field-assisted etching rate of inner pore becomes slower, leading to the shorter nanotube length and denser ribs on the outer wall surface. In addition, high water content helps the electrolyte to redissolve the top of NTAs through the etching reaction.^{37,38} Differences in the driving force for the growth and redissolution of NTAs explain why the water content controls the length and ribs of NTAs.

We investigated crystallization of the prepared NTAs using an in-situ XRD with increasing temperature. Thermal annealing up to 450 °C didn't change the tubular shape, but led to slight shrinkage of the tube diameter (~ 5 nm), as similar to literatures.³⁹ The XRD results (Fig. 2a-b) show only Ti peaks

from the as-grown NTAs, indicating they are amorphous, which is also evidenced by HRTEM analysis (see Fig. S1, ESI[†]). With increasing temperature, XRD peaks for the (101), (004), and (200) planes of TiO₂ anatase structure evolve out from all NTA samples, which starts at 285~290 °C. The crystallization of the 2W-NTAs begins at slightly lower temperature than the 5W-NTAs. In 2W-NTAs, (004) peak is much stronger than (200) peak. This means that the 2W-NTAs are p-NTAs which are composed of anatase grains in which (004) planes preferentially orient to the vertical direction of the substrate. On the other hand, the XRD pattern of 5W-NTAs is similar to that of randomly oriented TiO₂ anatase polycrystalline films, indicating that 5W-NTA is r-NTA.^{40,41} This significant dependence of the crystallographic structure on the water content is observed even in the early crystallization stage. The p-NTAs and the r-NTAs exhibit a different intensity ratio of (004) to (200) peaks at ~290 °C. As plotted in Fig. 2c, different peak intensity ratio of p-NTAs and r-NTAs is maintained until 450 °C. Therefore, it can be deduced that the crystallization with or without the preferred orientation diverges from the beginning of the phase transformation. The preferred-orientation found in XRD patterns is confirmed by TEM study (see Fig. S2, ESI[†]). The HRTEM images of NTAs annealed at 450 °C for 1 hr show that the axis of 2W-NTAs is parallel to <001> of anatase and 5W-NTAs are randomly oriented. In addition, the r-NTAs are composed of fine grains with the size of ~5 nm, while the p-NTAs are composed of much larger grains which size is very challenging to be estimated because of low angle boundaries. For an example, a dark field image of the p-NTAs shows that nearby grains have similar orientations so that the

agglomerate looks like a single domain as large as a few hundreds of nanometer (see Fig. S3, ESI[†]).

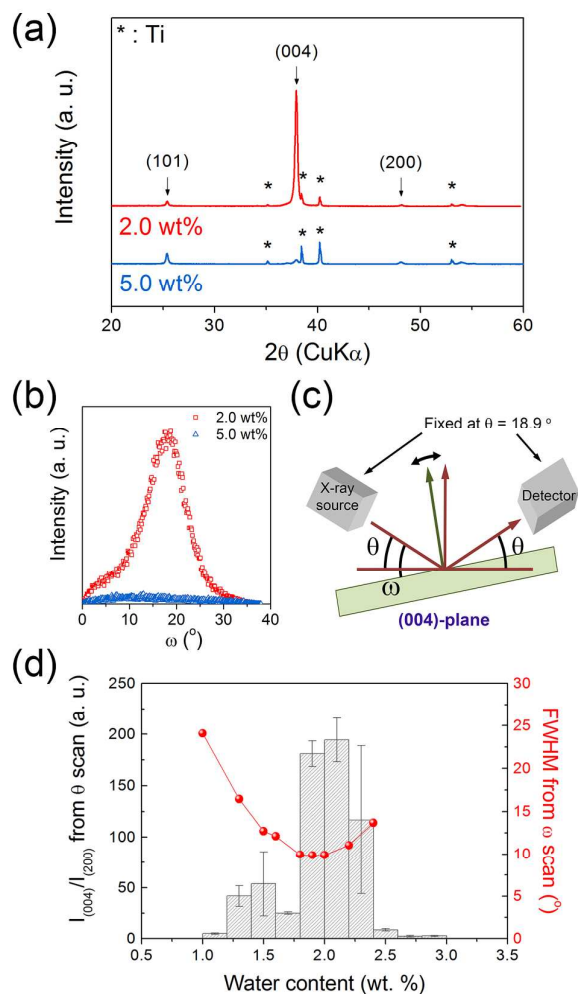


Fig. 4. (a) X-ray diffraction (θ - 2θ scan) patterns, and (b) rocking curves (ω scan) of the 2.0W-TiO₂ NTAs and 5.0W-TiO₂ NTAs. (c) Illustration showing the principle of the ω scan. (d) Histogram (left axis) presenting the peak intensity ratios $I_{(004)}/I_{(200)}$ calculated from (a), and FWHM (right axis) of the rocking curves derived from (b). FWHM of the samples grown with the water contents of > 2.5 wt% cannot be estimated because of very weak and broad curves.

To understand the evolution of preferred orientation, we studied the initial stage of the crystallization paths to p-NTA and r-NTA using TEM. We picked up partially crystallized NTAs where the amorphous phase and the anatase phase were mixed. For this purpose, as-anodized 2W-NTAs and 5W-NTAs were annealed at 290 °C for 1 hr, because the crystallization from amorphous to anatase phase started between 285 °C and 290 °C (see Fig. 2a-b). Fig. 3 shows the cross-sectional TEM images and fast Fourier transform (FFT) patterns of the partially-crystallized nanotubes from the p-NTAs, and the r-NTAs. In case of the p-NTA, aligned lattice patterns are found only in the region near the outer surface. In case of the r-NTA, however, the inner part of the nanotubes shows obvious local

fluctuation of the contrast (see Fig. 3e) and formation of small crystallized islands. To investigate a detailed crystal structure, we obtained FFT patterns from the Fig. 3b and Fig. 3f, as shown in Fig. 3c and Fig. 3g. In case of the p-NTA, the FFT patterns of A, B, and C region are exactly same; only vertically placed dots corresponding to the $\{200\}$ planes are found. Therefore, the dark color region near an outer wall surface is an anatase single grain oriented along the $[001]$ direction. On the other hand, the FFT pattern of D region indicates that the rest of nanotube wall remains as amorphous. It demonstrates that the crystallization of p-NTA is triggered at the wall surface and the crystal domain grows toward the inner wall, leading to the $[001]$ -preferred orientation along the longitudinal direction of nanotube. Whereas, the anatase crystallites in r-NTA (dark regions in Fig. 3f) are sporadically distributed in the amorphous medium (bright regions) located between the inner and outer walls of the NTAs. In addition, the FFT patterns of crystallites (E and F regions) are not indexed as only $\{200\}$ planes, and show different orientations. TEM results of r-NTA demonstrate that the multiple nucleation and growth of anatase crystals in the nanotube walls are responsible for the randomly oriented tiny grains. Fig. 3d and 3h schematically describe pathways toward the p-NTA and the r-NTA.

We previously reported that ~ 2 wt% of water content leads to the preferred orientation.²⁶ In this study, we performed more systematic research to examine the effect of water content on the degree of preferred orientation and find a water content window for optimizing the preferred orientation of NTAs. Water content in the electrolyte was accurately varied from 1.0 wt% to 3.0 wt% with 0.2 wt% intervals, and to 10.0 wt% with 2.0 wt% intervals, distinct from the above works where the water content (wt%) was controlled in the ones place. To reduce the uncertainty associated with measuring the water content down to the one decimal place, we used the batch size of 1000 mL when the electrolyte was prepared. In this case, 0.1 wt% water in the electrolyte equals to ~ 1 mL water so that the experimental result was more reproducible. Representative XRD patterns (θ - 2θ), and rocking curves (ω -scan) of (004) peaks of annealed NTAs (2.0W-NTAs and 5.0W-NTAs) are shown in Fig. 4a and 4b, respectively. The rocking curves were measured by rocking the sample. The location of X-ray source and the detector is fixed so that they can detect only Bragg peak for the (004) plane of anatase structure (Fig. 4c). This geometry of the source and the detector enabled us to examine the tilting of (004) plane of grains from the substrate surface plane. The peak intensity ratio $I_{(004)}/I_{(200)}$ from the θ - 2θ scan, and the full width half maximum (FWHM) values from the ω -scan are plotted in Fig. 4d, as a function of water content in the electrolyte. The $I_{(004)}/I_{(200)}$ ratio dramatically increases at 1.0-2.0 wt%, and reaches to the maximum at 2.0-2.2 wt%, with an extremely high value ~ 200 , and then dramatically reduced to ~ 1 for water content > 3.0 wt%. The FWHM value is minimum ($< 10^\circ$) for the water content of 2.0 wt% where the $I_{(004)}/I_{(200)}$ ratio is the largest. This result emphasizes the importance of the water content for the preferred orientation.

Based on the observations presented in this study and in previous reports, we suggest a possible mechanism for the formation of the p-NTAs and the r-NTAs. First, the crystallization starts at the outer wall surface in the p-NTA, which is attributed to the fact that fluorine is enriched near the outer surface of the nanotubes.^{33,42,43} Since the presence of F⁻ ion in amorphous TiO_x accelerates the crystallization of anatase TiO₂,⁴⁴ the fluorine-rich oxide at the outer wall crystallizes at lower temperature than the region near the inner wall. Second, the TiO₂ nucleus seeds formed on the outer surface of NTAs grow along [001],⁴⁵⁻⁴⁸ since {001} faces of the anatase phase has higher surface energy than {101} faces.^{49,50} Then, the anisotropic, preferred oriented nucleus grow into amorphous TiO₂ between inner and outer surfaces of the NTAs, leading to NTAs with the preferred orientation. On the other hand, in case of the r-NTA condition, this progressive grain growth does not happen, because of high content of hydroxyl group in the amorphous TiO₂. In the anodization process, water in the electrolyte is a source of oxygen for metal oxidation and provides OH⁻ ions into the amorphous TiO₂ layer.^{27,28} When the water content is too low, the O/Ti ratio of the anodic oxide is too small to form stoichiometric TiO₂.²⁷ The film grown in 0 wt% water condition has no pore structure and irregular shape, and rarely forms anatase phase (Fig. S4, ESI⁺).

In contrast, when the water content is higher than 2.5 wt% (according to our results), the anodic oxide layer contains a large amount of hydroxyl groups as well as oxygen.^{26,30,51,52} Moreover, the high water content results in rough outer walls with a number of ribs, which possesses more OH⁻ ions and less F⁻ ions than the smooth wall because the ribs are formed by the electric field-assisted dissolution. The hydroxyl groups in the amorphous TiO_x reduce an energy barrier for the crystallization, since they facilitate the crystallization of the amorphous TiO₂ via a polycondensation reaction.⁵³⁻⁵⁵ Therefore, the crystallization starts at multiple sites between outer and inner surfaces of NTAs, which is responsible for the formation of randomly oriented fine grains in r-NTAs.

Relatively large, preferred-oriented grains of p-NTAs are expected to improve a charge transport property compared to randomly oriented grains of r-NTAs. In our previous study, we demonstrated ~ two times faster electron transport in a dye-sensitized solar cell system, using p-NTAs showing the XRD peak intensity ratio ($I_{(004)}/I_{(200)}$) of ~20.²⁶ Faster electron transport of the p-NTAs photoelectrode, which led to a longer electron diffusion length, induced excellent photovoltaic current density. In the present work, we investigated electrical properties of the p-NTAs, which shows the $I_{(004)}/I_{(200)}$ as much as ~200. Fig. 5 shows the local current-voltage (*I-V*) curves for the p-NTAs and r-NTAs, measured by c-AFM. Pt/TiO₂/Ti diodes were formed using the p-NTAs (length: 10 μm) and r-NTAs (length: 10 μm) on Ti substrates by an AFM tip coated with Pt film. The p-NTAs have higher forward current compared with the r-NTA. From the obtained *I-V* curve, their series resistance (R_s) are determined using the following equation:⁵⁶

$$I = AA^*T^2 \exp\left(-\frac{q\Phi_b}{kT}\right) \exp\left(-\frac{q(V - IR_s)}{nkT}\right)$$

where A is the diode area, A^* is the effective Richardson constant, I is the current and V is the applied voltage. Calculated ideality factor (n) of p-NTA and r-NTA were 8.82 and 6.46, respectively. The series resistance (R_s) of the p-NTA ($R_s = 47.2 \text{ k}\Omega$) is five times lower than that of the r-NTA ($R_s = 243.3$

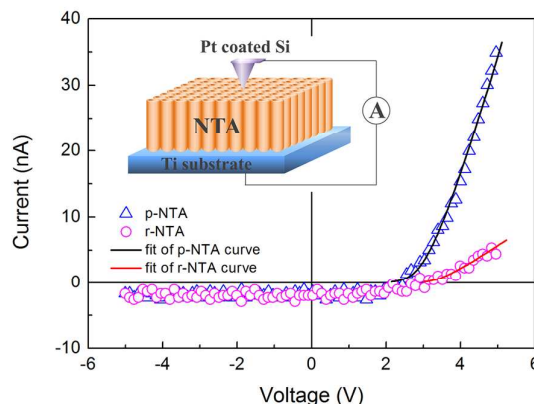


Fig. 5. *I-V* curves measured by c-AFM, for p-NTA (2.0 wt%) and r-NTA (5.0 wt%). Inset illustrates the measurement.

$\text{k}\Omega$). The lower resistance of the p-NTA is interpreted in terms of the orientation difference between the p-NTA and the r-NTA. The p-NTAs are composed of low angle grain boundary, which allows faster electron transport.^{17,57} Furthermore, large grain size of the p-NTA reduces an areal density of grain boundaries which acts as a scattering center.^{12,18} Consequently, the electron trapping and phonon generation are considered to be significantly retarded in the preferred-orientation optimized NTAs, which implies that the preferred-orientation optimized NTAs can improve the performances of TiO₂ NTA-based electronic, optoelectronic, photovoltaic, and battery devices.

4. Conclusion

We investigated the effect of the water content in the electrolyte on the crystallization behavior of the anodic TiO₂ NTAs, during the annealing process. It is found that the water content is critical to appearance of anatase TiO₂ NTAs with the preferred orientation. Effects of water can be summarized as follows. First, water in the electrolyte affects the morphology of the as-grown NTAs, which is attributed to the different electric-field assisted oxidation on the surface of the metal substrate, hence the thickness of the oxide barrier layer. Second, NTAs grown in 1.5-2.5 wt% water transform from amorphous to p-NTAs, while the NTAs grown with > 2.5 wt% of water content transform to r-NTAs. More importantly, in the p-NTAs, crystallization starts from the outer wall of nanotubes due to lower crystallization barrier of F ion-rich amorphous TiO₂, leading to the formation of a thin layer along the

nanotube surface. On the other hand, in the r-NTAs, nucleation starts inside of nanotubes sporadically without preferred orientation. Larger amount of hydroxyl ions inside NTAs results in multiple nucleation over nanotubes wall in the NTAs grown in high water content conditions (> 3.0 wt%). The resistance of p-NTAs is only 20% as small as that of r-NTAs, since large grains and low angle boundaries of p-NTAs suppress electron scattering. The superior carrier transport of p-NTAs is expected to improve the performance of many device systems such as solar cells and Li-ion batteries.

Acknowledgements

This work was supported by National Science Foundation, US (Grant No. CMMI-1333182) and the Global Frontier R&D Program on Center for Multiscale Energy System funded by the National Research Foundation under the Ministry of Science, ICT & Future Planning, Korea (2012M3A6A7054855).

Notes and references

- J. W. Diggle, T. C. Downie, and C. W. Goulding, *Chem. Rev.*, 1969, **69** (3), 365.
- W. Lee, K. Schwirn, M. Steinhart, E. Pippel, R. Scholz, and U. Gösele, *Nature Nanotech.*, 2008, **3**, 234.
- W. Wei, J. M. Macak, N. K. Shrestha, and P. Schmuki, *J. Electrochem. Soc.*, 2009, **156**, K104.
- N. K. Allam, X. J. Feng, and C. A. Grimes, *Chem. Mater.*, 2008, **20**, 6477.
- I. Sieber, H. Hildebrand, A. Friedrich, and P. Schmuki, *Electrochem. Commun.*, 2005, **7**, 97.
- J. Z. Ou, R. A. Rani, M. H. Ham, M. R. Field, Y. Zhang, H. Zheng, P. Reece, S. Zhuiykov, S. Sriram, M. Bhaskaran, R. B. Kaner, and K. Kalantar-zadeh, *ACS Nano*, 2012, **6**, 4045.
- N. Mukherjee, M. Paulose, O. K. Varghese, G. K. Mor, and C. A. Grimes, *J. Mater. Res.*, 2003, **18**, 2296.
- G. K. Mor, O. K. Varghese, M. Paulose, and C. A. Grimes, *Adv. Funct. Mater.*, 2005, **15**, 1291.
- J. M. Macak, S. Aldabergerova, A. Ghicov, and P. Schmuki, *Phys. Stat. Sol.* 2006, **203**, R67.
- G. K. Mor, K. Shankar, M. Paulose, O. K. Varghese, and C. A. Grimes, *Nano Lett.*, 2006, **6**, 215.
- J. M. Macak, H. Tsuchiya, L. Taveira, S. Aldabergerova, and P. Schmuki, *Angew. Chem. Int. Ed.*, 2005, **44**, 7463.
- K. Zhu, N. R. Neale, A. F. Halverson, J. Y. Kim and A. J. Frank, *J. Phys. Chem. C*, 2010, **114**, 13433.
- W.-T. Sun, Y. Yu, H.-Y. Pan, X.-F. Gao, Q. Chen, and L.-M. Peng, *J. Am. Chem. Soc.*, 2008, **130**, 1124.
- W. Wei, G. Oltean, C.-W. Tai, K. Edstrom, F. Bjorefors, and L. Nyholm, *J. Mater. Chem. A*, 2013, **1**, 8160.
- Q. Zheng, B. Zhou, J. Bai, L. Li, Z. Jin, J. Zhang, J. Li, Y. Liu, W. Cai, and X. Zhu, *Adv. Mater.*, 2008, **20**, 1044.
- A. J. Frank, N. Kopidakis and J. van de Lagemaat, *Coord. Chem. Rev.*, 2004, **248**, 1165.
- W. Choi, J.-K. Lee and A. T. Findikoglu, *Appl. Phys. Lett.*, 2006, **89**, 262111.
- H. S. Jung, J.-K. Lee, J. Lee, B. S. Kang, Q. Jia, M. Nastasi, J. H. Noh, J.-M. Cho and S. H. Yoon, *Langmuir*, 2008, **24**, 2695.
- C. Richter, and C. A. Schmittenmaer, *Nat. Nanotechnol.*, 2010, **5**, 769.
- O. K. Varghese, M. Paulose, and C. A. Grimes, *Nat. Nanotechnol.*, 2009, **4**, 592.
- S. Guldin, S. Huttner, P. Tiwana, M. C. Orillall, B. Ulgut, M. Stefik, P. Docampo, M. Kolle, G. Divitini, C. Ducati, S. A. T. Redfern, H. J. Snaith, U. Wiesner, D. Eder, and U. Steiner, *Energy Environ. Sci.*, 2011, **4**, 225.
- E. J. W. Crossland, N. Noel, V. Sivaram, T. Leijtens, J. A. Alexander-Webber, and H. J. Snaith, *Nature*, 2013, **495**, 215.
- M. Kim, C. Bae, H. Kim, H. Yoo, J. M. M. Moreno, H. S. Jung, J. Bachmann, K. Nielsch, and H. Shin, *J. Mater. Chem.*, 2013, **1**, 14080.
- J. Zhao, X. Wang, T. Sun, and L. Li, *Nanotechnology*, 2005, **16**, 2450.
- M.-H. Jung, M.-J. Chu, M. G. Kang, *Chem. Commun.*, 2012, **48**, 5016.
- S. Lee, I. J. Park, D. H. Kim, W. M. Seong, D. W. Kim, G. S. Han, J. Y. Kim, H. S. Jung, and K. S. Hong, *Energy Environ. Sci.*, 2012, **5**, 7989.
- H. E. Prakasam, K. Shankar, M. Paulose, O. K. Varghese, and C. A. Grimes, *J. Phys. Chem. C*, 2007, **111**, 7235.
- W. Wei, S. Berger, C. Hauser, K. Meyer, M. Yang, and P. Schmuki, *Electrochem. Commun.*, 2010, **12**, 1184.
- Y.-M. Li, and L. Young, *J. Electrochem. Soc.*, 2001, **148**, B337.
- W. M. Seong, D. H. Kim, I. J. Park, G. D. Park, K. Kang, S. Lee, K. S. Hong, *J. Phys. Chem. C*, 2015, **119**, 13297.
- S. P. Albu, A. Ghicov, J. M. Macak, and P. Schmuki, *Phys. Status Solidi RRL*, 2007, **1**, R65.
- S. P. Albu, A. Ghicov, and P. Schmuki, *Phys. Status Solidi RRL*, 2009, **3**, 64.
- H. Habazaki, K. Fushimi, K. Shimizu, P. Skeldon, and G. E. Thompson, *Electrochem. Commun.* 2007, **9**, 1222.
- A. Valota, D. J. LeClere, P. Skeldon, M. Curioni, T. Hashimoto, S. Berger, J. Kunze, P. Schmuki, and G. E. Thompson, *Electrochim. Acta*, 2009, **52**, 4321.
- K. S. Raja, T. Gandhi, and M. Misra, *Electrochem. Commun.* 2007, **9**, 1069.
- P. Roy, S. Berger, and P. Schmuki, *Angew. Chem. Int. Ed.*, 2011, **50**, 2904.
- H. Yin, H. Liu, and W. Z. Shen, *Nanotechnology*, 2010, **21**, 035601.
- S. Berger, J. Kunze, P. Schmuki, A. T. Valota, D. J. LeClere, P. Skeldon, and G. E. Thompson, *J. Electrochem. Soc.*, 2010, **157**, C18.
- S. P. Albu, H. Tsuchiya, S. Fujimoto, and P. Schmuki, *Eur. J. Inorg. Chem.*, 2010, **2010**, 4351.
- S. Lee, I.-S. Cho, J. H. Lee, D. H. Kim, D. W. Kim, J. Y. Kim, H. Shin, J.-K. Lee, H. S. Jung, N.-G. Park, K. Kim, M. J. Ko, and K. S. Hong, *Chem. Mater.*, 2010, **22**, 1985.
- J. R. McCormick, B. Zhao, S. A. Rykov, H. Wang, and J. G. Chen, *J. Phys. Chem. B*, 2004, **108**, 17398.
- K. Yasuda, J. M. Macak, S. Berger, A. Ghicov, and P. Schmuki, *J. Electrochem. Soc.*, 2007, **154**, C472.
- J. M. Macak, H. Tsuchiya, A. Ghicov, K. Yasuda, R. Hahn, S. Bauer, and P. Schmuki, *Curr. Opin. Solid State Mater. Sci.*, 2007, **11**, 3.
- J. Yu, G. Dai, and B. Cheng, *J. Phys. Chem. C*, 2010, **114**, 19378.
- Y. X. Zhang, G. H. Li, Y. X. Jin, Y. Zhang, J. Zhang, and L. D. Zhang, *Chem. Phys. Lett.*, 2002, **365**, 300.
- R. A. Caruso, J. H. Schattka, and A. Grenier, *Adv. Mater.*, 2001, **13**, 1577.
- Y. Lei, L. D. Zhang, G. W. Meng, G. H. Li, X. Y. Zhang, C. H. Liang, W. Chen, and S. Z. Wang, *Appl. Phys. Lett.*, 2001, **78**, 1125.
- B. Xiang, Y. Zhang, Z. Wang, X. H. Luo, Y. W. Zhu, H. Z. Zhang, and D. P. Yu, *J. Phys. D*, 2005, **38**, 1152.
- J.-N. Nian, and H. Teng, *J. Phys. Chem. B*, 2006, **110**, 4193.
- H. G. Yang, C. H. Sun, S. Z. Qiao, J. Zou, G. Liu, S. C. Smith, H. M. Cheng, and G. O. Lu, *Nature*, 2008, **453**, 638.

ARTICLE

Journal Name

- 51 B. Melody, T. Kinard, and P. Lessner, *Electrochem. Solid State Lett.*, 1998, **1**, 126.
- 52 G. M. Krembs, *J. Electrochem. Soc.*, 1963, **8**, 938.
- 53 K. Yanagisawa, and J. Ovenstone, *J. Phys. Chem. B*, 1999, **103**, 7781.
- 54 M. Fernandez-Garcia, X. Wang, C. Belver, J. C. Hanson, and J. A. Rodriguez, *J. Phys. Chem. C*, 2007, **111**, 674.
- 55 S. G. Kumar, and K. S. R. K. Rao, *Nanoscale*, 2014, **6**, 11574.
- 56 M. Saglam, E. Ayyddiz, A. Gumus, A. Turut, H. Efeoglu, and S. Tuzemen, *Appl. Phys. A*, 1996, **62**, 269.
- 57 A. T. Findikoglu, W. Choi, V. Matias, T. G. Holesinger, Q. X. Jia, and D. E. Peterson, *Adv. Mater.*, 2005, **17**, 1527.